Talanta 302 (2026) 129444

Contents lists available at ScienceDirect

Talanta

journal homepage: www.elsevier.com/locate/talanta

Frequency-resolved characterization of thin-layer solid-contact ion-selective electrodes: Deconvoluting electron and ion transfer with AC voltammetry

Gregorio Laucirica [a,1], Nuria Martínez-Lorca [a,1], Gastón A. Crespo [a,b], María Cuartero [a,b,*]

[a] UCAM-SENS, Universidad Católica San Antonio de Murcia, UCAM HiTech, Avda. Andres Hernandez Ros 1, 30107, Murcia, Spain
[b] Department of Chemistry, School of Engineering Science in Chemistry, Biochemistry and Health, KTH Royal Institute of Technology, Teknikringen 30, SE-114 28, Stockholm, Sweden

ARTICLE INFO

Keywords:
Poly(3-octylthiophene)
Membranes
Ion-selective electrode
Thin-layer
AC voltammetry
Charge transfer

ABSTRACT

This work investigates the coupled electron–ion transfer (ET–IT) phenomena occurring in solid-contact ion-selective electrodes based on a poly(3-octylthiophene) (POT) film backside contacted with a plasticized nanomembrane through cyclic voltammetry (CV), electrochemical impedance spectroscopy (EIS), and alternating current voltammetry (ACV). The CVs presented the typical thin-layer behavior, whereas EIS revealed distinct regions corresponding to membrane resistance, charge transfer, and capacitive responses, allowing for the separation and quantification of the ET–IT contributions. The analysis by electrical equivalent circuit demonstrated that, as the potential approaches the redox peak, the membrane resistance markedly increases from 2.6 kΩ to 40 kΩ due to ion expulsion. Charge transfer resistance followed the "v"-shaped dependence expected for thin-layer systems, with a minimum at 0.86 kΩ. Time constant analysis confirmed that ionic dynamics were significantly faster than electron transfer processes. Building on this insight, ACV was used to bridge the spectral deconvolution capability of EIS with the simplicity of CV. The ACV responses were found to strongly depend on frequency. At low frequencies (<10 Hz), the signals were dominated by faradaic ET–IT peaks; while at higher frequencies (>250 Hz), the response transitioned to a sigmoidal profile governed by ion transport and membrane resistance. This frequency selectivity enabled distinguishing between ions of different lipophilicity (e.g., Na^+ vs. TBA^+) in membranes exclusively containing a cation exchanger, demonstrating ion-specific peak shifts when using ionophore-based membranes (e.g., valinomycin for K^+). Finally, the possibility of determining signal changes with variations of the K^+ concentration in the nanomolar range by employing CV and ACV, together with a comparison of the sensing performance with both techniques, was demonstrated.

1. Introduction

The need for rapid, reliable, and decentralized analysis has intensified the search for sensing platforms that can operate outside of centralized laboratories [1,2]. In this context, electrochemical sensors stand out due to their inherent advantages, including low cost, portability, and miniaturization, as well as minimal instrumentation requirements and the ability to provide real-time results [3,4]. These features, combined with the versatility of electrochemical sensors, make them suitable for a wide range of applications, including point-of-care analysis, environmental monitoring, and food safety, among others [5–7]. Within the broad spectrum of electrochemical sensors, ion-selective electrodes (ISEs) have played a central role in chemical analysis for more than half a century [8–10]. The classical inner-filling potentiometric ISEs, which rely on a liquid electrolyte between a sensing membrane and an internal reference electrode, have become standard tools in analytical practices for ions' detection. For instance, the glass pH electrode has become indispensable in routine laboratory practice, industrial quality control, and fieldwork alike [11]. However, inner-filling ISEs suffer from drawbacks inherent to their liquid internal contact. Issues such as evaporation, leakage, limited mechanical stability, and challenges in miniaturization restrict their versatility.

* Corresponding author. Department of Chemistry, School of Engineering Science in Chemistry, Biochemistry and Health, KTH Royal Institute of Technology, Teknikringen 30, SE-114 28, Stockholm, Sweden.
mariacb@kth.se (M. Cuartero)
[1] These authors contributed equally to the work.

https://doi.org/10.1016/j.talanta.2026.129444
Received 12 December 2025; Received in revised form 15 January 2026; Accepted 20 January 2026
Available online 22 January 2026

The development of all-solid-contact ion-selective electrodes (SC-ISEs) represented a significant advancement in addressing the limitations of traditional ISEs [12–14]. By replacing the liquid inner filling with a solid-state electron–ion transducer and employing plasticized polymeric membranes, these devices preserve the potentiometric principle while overcoming many of the weaknesses of their predecessors. Typical electron–ion transducers include electroactive polymers [15–17], and high-surface-area high-capacity materials [18], which provide stable ion-to-electron charge conversion. Plasticized polymeric membranes generally consist of a polymer matrix (e.g., polyvinyl chloride (PVC) or polyurethane), plasticizer (e.g., bis(2-ethylhexyl) sebacate, DOS), cation exchanger (e.g., sodium tetrakis[3, 5-bis-(trifluoromethyl)phenyl]borate, NaTFPB), and ionophore that serves as the ion-selective recognition element (e.g., valinomycin for K^+-selective SC-ISEs). Importantly, the absence of internal solutions enables miniaturization and improves durability, which broadens the applicability of ISEs. Thus, SC-ISEs have given rise to a variety of novel electrode configurations, each adapted to specific analytical needs. Membranes with thicknesses of a few micrometers have been integrated into diverse architectures such as paper-based electrodes [19,20], microneedles for ion monitoring in interstitial fluid and plants [21,22], submersible probes for water analysis [23], and nanopipettes for single-cell measurements [24]. This versatility highlights not only the robustness of the all-solid-contact concept but also its potential to transform ISE technology into a truly universal platform for in situ ions' monitoring.

Recent advances have pushed membrane design to the nanoscale, reducing its thickness to just a few hundred nanometers [25,26]. This innovation has generated the so-called thin-layer voltammetric SC-ISEs, which exhibit unique properties compared to their potentiometric counterparts. The thin-layer configuration of the membrane confines ion transport within the nanoscale film, which dramatically reduces the membrane resistance, enabling the use of dynamic electrochemical methods that enhance the sensing sensitivity [27]. Moreover, these electrodes have demonstrated the potential for calibration-free operation, a long-standing goal in analytical chemistry, as well as the capability to perform multi-ion detection with a single electrode by exploiting distinct voltammetric signatures [28–30]. These breakthroughs have quickly positioned thin-layer voltammetric ISEs at the forefront of electrochemical ion sensing research.

Despite their impressive features, the operation mechanism of thin-layer ISEs remains highly nontrivial. Their function depends critically on the coupling between electron transfer (ET) at the solid contact and ion transfer (IT) across the ultrathin ion-selective membrane. For example, in voltammetric SC-ISEs built with poly(3-octylthiophene) (POT) acting as the solid-contact and a plasticized PVC-based

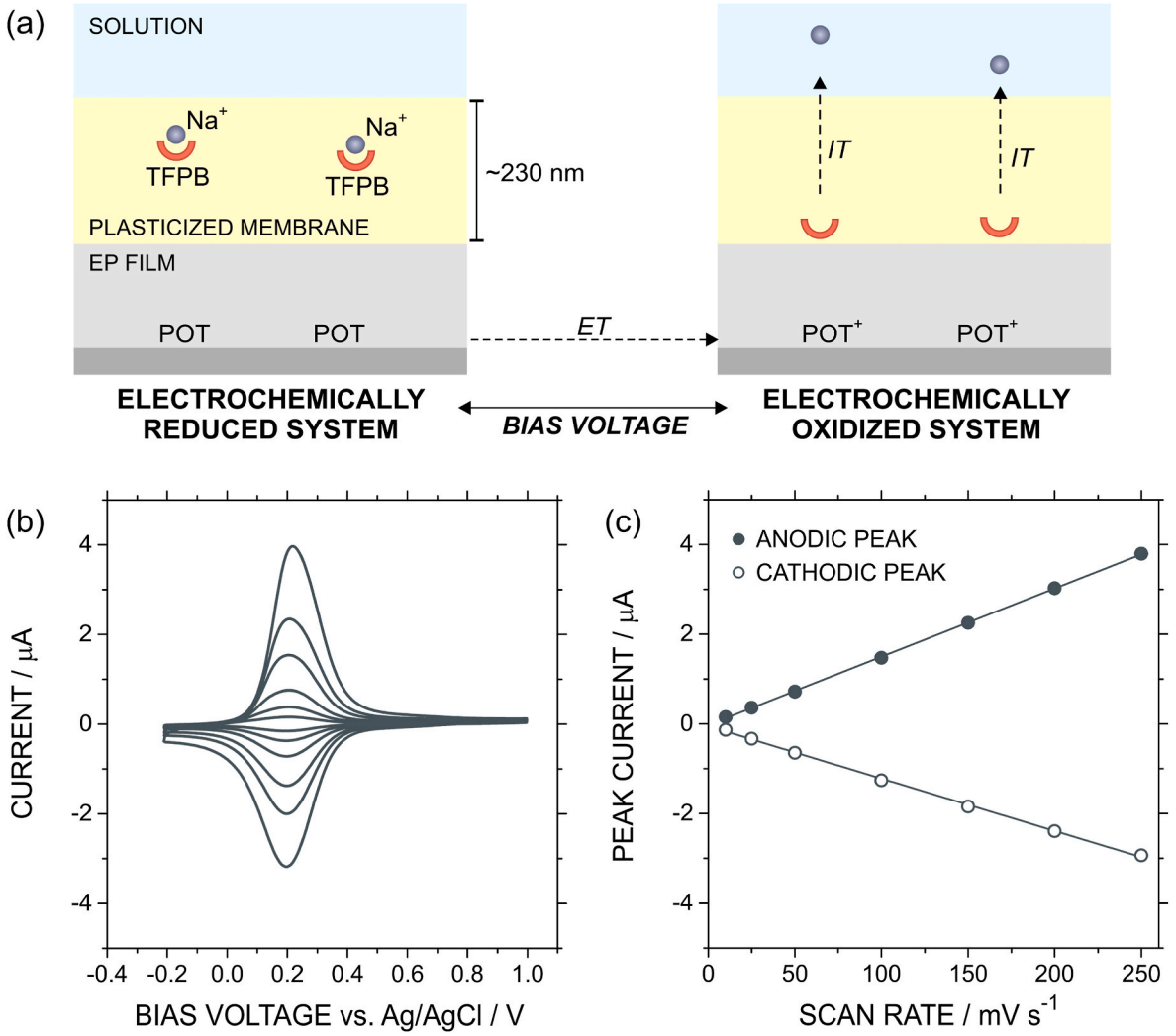

Fig. 1. (a) Scheme illustrating the coupled ET-IT in an SC-ISE based on a POT film and plasticized membrane without ionophore. EP, ET, and IT refer to electroactive polymer, electron transfer, and ion transfer, respectively. (b) Voltammograms and (c) peak currents at different scan rates. In all cases, the supporting electrolyte was 10 mM NaCl, and the SC-ISE was GC/POT/MI.

nanomembrane containing a cation exchanger (and optionally ionophore), the following sequence occurs: when POT is in its reduced state, the film is uncharged, the membrane retains its fixed ionic sites (from the cation exchanger) and equilibrates with ions entering from the sample solution (Fig. 1a) [26,31]. Upon oxidation of POT (ET process), due to the application of a proper bias voltage, positive charges are formed on the polymer backbone and, to preserve electroneutrality, cations are expelled from the membrane into the solution (IT process). Conversely, when a reducing potential is re-applied, the POT redox transformation removes the charged sites, and cations are taken up again into the membrane. It is worth mentioning that this fast electroneutrality-driven balance, which enables reversible and well-defined peaks (without side reactions) depending on the concentration of non-redox ions, together with its high potential stability and easy integration on the electrode surface (via electropolymerization or drop-casting), makes POT one of the most widely used electroactive polymers in voltammetric SC-ISEs [31–33].

This reversible ET-IT process is typically manifested in cyclic voltammetry (CV) as a discernible pair of Gaussian-shaped redox peaks [34,35]. In these cases, the peak area reflects the total number of ions present in the membrane, which is related to the membrane's cation exchange capacity [36]. In contrast, the peak position is influenced by the lipophilicity and by the interactions between the mobile ions and the membrane components, including the cation exchanger and the ionophore [30]. Notably, the ET–IT coupling is highly system-dependent, which makes it difficult to generalize findings across different transducers, ionophores, or ionic species. This challenge, compounded by the complexity of disentangling the multiple processes occurring at the different interphases and phases, hampers both the rationalization of the observed behavior and the subsequent optimization of device performance. To bridge these knowledge gaps, significant efforts have been devoted to characterizing these systems through electrochemical techniques such as CV, chronoamperometry, and computational modeling, which have provided valuable but often fragmentary insights [37–39].

Electrochemical impedance spectroscopy (EIS) analysis has been widely employed in the sensor field [40,41] and has more recently emerged as a powerful approach for investigating thin-layer systems [42–44]. The distribution of relaxation times (DRT) applied to EIS data enabled the deconvolution of overlapping processes, revealing the distinct contributions of charge transfer, ion diffusion/migration, and capacitive elements in an ISE electrode based on POT and a plasticized polymeric nanomembrane [45]. This methodology provided one of the first systematic demonstrations of how relaxation time distributions can be leveraged to rationalize the dynamics of ET-IT coupling in thin-layer ISEs. Nevertheless, the approach is not without limitations: the divergence of impedance at low frequencies typical of thin-layer systems (i.e., imaginary component of impedance, $Z_{IM} \rightarrow \infty$ as frequency approaches 0 Hz) complicates the interpretation of DRT spectra, posing a barrier to extracting qualitative and quantitative parameters with full reliability [46].

Motivated by these limitations, the present work aims to develop a complementary, frequency-resolved experimental strategy that enables a straightforward interrogation of ET-IT processes in thin-layer solid-contact ISEs. To this end, we combine CV, EIS, and AC voltammetry at various frequencies to disentangle the mechanisms of ET and IT in an ISE based on POT in contact with plasticized PVC membranes of different characteristics. Our study not only provides a deeper understanding of the fundamental processes governing the operation of the ISEs, but it also evaluates the analytical implications of these insights. Effectively, we demonstrate how advanced frequency-domain methods can guide the rational design of thin-layer ISEs, which is crucial for enabling enhanced sensitivity, multi-ion detection, and ultimately, more reliable decentralized, robust sensing solutions.

2. Experimental

Reagents and instrumentation. 3-octylthiophene (97 %), selectophore high molecular weight poly(vinyl chloride) (PVC), anhydrous tetrahydrofuran (≥99.9 %, THF), Tetra-*n*-butylammonium chloride (≥95 %, TBACl), sodium tetrakis[3,5-bis-(trifluoromethyl)phenyl] borate (NaTFPB), bis(2-ethylhexyl)sebacate (DOS), potassium ionophore I (Valinomycin), sodium hypochlorite solution (6–14 %) and high purity grade sodium chloride (99.99 %, NaCl) were obtained from Sigma Aldrich. Potassium chloride (99.5 %, KCl) and anhydrous acetonitrile (≥99.5 %), were purchased from VWR, while anhydrous lithium perchlorate (99 %, $LiClO_4$) was provided by Thermo Scientific. All reagents were employed without any further treatment. All aqueous solutions were prepared in deionized MQ® water (>18.2 MΩ cm).

All electrochemical experiments were conducted in a three-electrode cell using a glassy carbon (GC) electrode (geometric area of 0.07 cm^2) and a Pt rod (geometric area >0.5 cm^2) from Metrohm Nordic (Stockholm, Sweden) as the working electrode and counter electrode, respectively. The reference electrode was a homemade Ag/AgCl wire prepared by immersing an Ag wire (0.5 mm) in a 1 % solution of sodium hypochlorite for 2 h. The electrodes were separated by 0.5 cm from each other and connected to an Autolab PGSTAT302 N potentiostat with SCAN250 and FRA32 modules from Metrohm Nordic. The electrochemical routines were applied by operating the potentiostat with the software provided by Metrohm Nordic, NOVA 2.1.

CVs were typically performed from −0.2 V to 1 or 1.2 V at a scan rate of 100 mV s^{-1}, otherwise mentioned. EIS spectra were recorded in the range of frequencies from 1×10^5 Hz to 0.1 Hz, measuring ten points per decade. In all the cases, a sinusoidal perturbation of ±10 mV was superimposed on a given direct current potential (E_{DC}). Before the measurement, the electrode was stabilized to the E_{DC} value by setting this voltage value for 10 s. To evaluate the contribution of the electron transfer, E_{DC} was fixed at the medium peak potential $E_{1/2,}$ which was calculated as the average of the oxidation and reduction peak potentials in the CV.

AC voltammograms were obtained by applying a staircase function from −0.2 V to 1 or 1.2 V. The total time of the step was 1.2 s, where 0.7 s corresponded to the application of a sine wave with a certain frequency and an amplitude of 25 mV. In all the cases, the scan rate was 8.4 mV s^{-1}. Measurements involving sine waves with frequencies >250 Hz required the use of the FRA32 module of the potentiostat. For AC voltammetry, the use of very small amplitudes (5–10 mV), as those typically required in EIS analysis, is not strictly necessary [47]. However, the comparison of EIS at amplitudes of 10 and 25 mV demonstrated differences <2 % in the impedance values (not shown), which could indicate a significant conservation of the linearity in this range of amplitudes [42,43]. In particular, higher amplitudes amplify the signal at the expense of a broadening of the peak that can lead to the loss of resolution.

Preparation of the thin-layer SC ISE. The SC-ISE consisted of POT as the ion-to-electron transducer and a plasticized PVC membrane as the ion-selective building block. The electrode preparation involved two steps: the POT electrosynthesis and PVC membrane deposition. First, the GC electrode was exposed to a mixture 0.1 M $LiClO_4$/0.1 M 3-octylthiophene in acetonitrile. The solution was degassed by fluxing N_2 for 15 min, and then, the POT was electropolymerized on the GC surface by performing two CV scans between 0 and 1.5 V (starting from 0 V) at 100 mV s^{-1}. Subsequently, the POT film was discharged by fixing the voltage at 0 V for 120 s. The film was thoroughly washed by immersing in acetonitrile and THF for 30 min and 10 s, respectively.

Then, the plasticized PVC membrane was deposited on the POT-modified GC electrode (GC/POT) by spin-coating. For this, the GC/POT electrode was first dried with a soft flow of nitrogen and then fixed in a rotating disk module (Metrohm Nordic). While the electrode rotated at 1500 rpm, 25 μL of a 1:4 dilution of a given cocktail was added to the electrode (Table 1). Under these conditions, the thickness of the resultant membrane is around ~230 nm, as revealed by our previous

Table 1
Composition of the membranes employed in this work. PVC and plasticizer amounts are expressed in wt.% of membrane. Cation exchanger (NaTFPB) and potassium ionophore (KI) are expressed in mmol kg^{-1} of membrane (M).

Membrane	PVC (wt. %)	%DOS (wt. %)	NaTFPB (mmol kg^{-1} M)	KI (mmol kg^{-1} M)
MI	33	66	40	–
MII	33	66	20	–
MIII	30	60	40	80

characterization by ellipsometry [48,49]. In all the cases, the cocktails were prepared and diluted by using anhydrous THF. The composition of these mixtures determines the features of the membrane and, in turn, the functionality of the SC-ISE. In the text, the different SC-ISEs are referred to as GC/POT/MX where MX indicates the cocktail employed for the membrane deposition.

3. Results and discussions

Fig. 1b shows the CV curves at different scan rates obtained for the SC-ISE GC/POT/MI electrode. In all the cases, the CV curve was characterized by a single pair of broad peaks centered at 0.2 V. The increment in the scan rate produced a linear increment in the anodic and cathodic peaks (Fig. 1c). This fact, together with the peak potential difference (anodic versus cathodic) below 5 mV at scan rates <100 mV s^{-1}, confirmed the presence of a thin-layer membrane with the typical behavior expected for redox probes adsorbed at the electrode surface. The peak width at half height of the peak at 205 mV for both the anodic and cathodic waves fairly exceeded the predicted value for an ideal one-electron thin-layer reaction of 90 mV [30,50,51]. This aspect was previously highlighted, with its origin being unknown yet. Electrodes modified with redox molecular systems have shown similar width peaks, which were attributed to slower kinetics, interaction between the different moieties in the film, among others [52–55]. On the other hand, at low scan rates, the anodic peak evidenced a sort of shoulder (Fig. S1), which could suggest the presence of additional polymer environment(s) requiring slightly different potentials to promote the redox reactions. All these aspects require a detailed analysis involving the use of various spectroscopic and electrochemical techniques, which is beyond the scope of this work.

As already mentioned, the redox switching in the GC/POT/MI electrode responsible for the pair of peaks in the CV consisted of the coupling of the redox reaction of the electroactive layer of POT and the ion uptake/expulsion of ions in the membrane. Thus, considering that MI presented only the cation exchanger NaTFPB (i.e., without an ionophore) and the background solution was composed only of NaCl, the oxidation of POT to POT^+ triggers the release of Na^+ from the membrane. In contrast, during reduction, the membrane uptakes Na^+ from the solution through the inverse process. With the aim of obtaining more detailed information, separating the contributions related to ion transport from those associated with the coupled ET–IT process, EIS measurements were performed at different $E_{DC,}$ and the results are provided in Fig. 2. To facilitate the analysis, the plots were divided according to their position regarding the half peak potential ($E_{1/2} \sim 0.19$ V).

Fig. 2a shows the Nyquist plots ($-Z_{IM}$ vs. Z_{REAL}) for E_{DC} in the range from −0.2 V to −0.02 V, *i.e.*, significantly lower than $E_{1/2}$. Under these conditions, POT is expected to be fully reduced and, consequently, the charged sites of the membrane due to the cation exchanger are neutralized by the presence of Na^+ ions provided by the supporting electrolyte. Notably, as the sinusoidal perturbation was minimal ±10 mV, no changes in the POT redox state were expected during the measurement, leading to a final EIS response with a negligible contribution of redox switching (faradaic signal). Among the four E_{DC} here evaluated, the EIS presented strong similarities. For instance, at high/moderate frequencies (10^5 to 10 Hz), the curves demonstrated a significant overlap with differences below 10 % between Z_{REAL} and $-Z_{IM}$ obtained at E_{DC} −0.2 V and −0.02 V. In all the cases, the Nyquist plot were characterized by two regions: a flat semicircle at moderate frequencies (10^5-$5x10^3$ Hz) and an abrupt increment in $-Z_{IM}$, proper of a capacitive behavior at moderate/low frequencies ($<5 \times 10^3$ Hz).

Region I at high/moderate frequencies did not appear in the bare GC nor GC/POT electrodes (see Fig. S2). Considering that, in addition to the fact that the semicircle features for that process were maintained constant across the different E_{DC} (when $E_{DC} \ll E_{1/2}$), this component was attributed to the membrane resistance. Such a resistance is expected to depend on several parameters, e.g., the mobility and number of charge

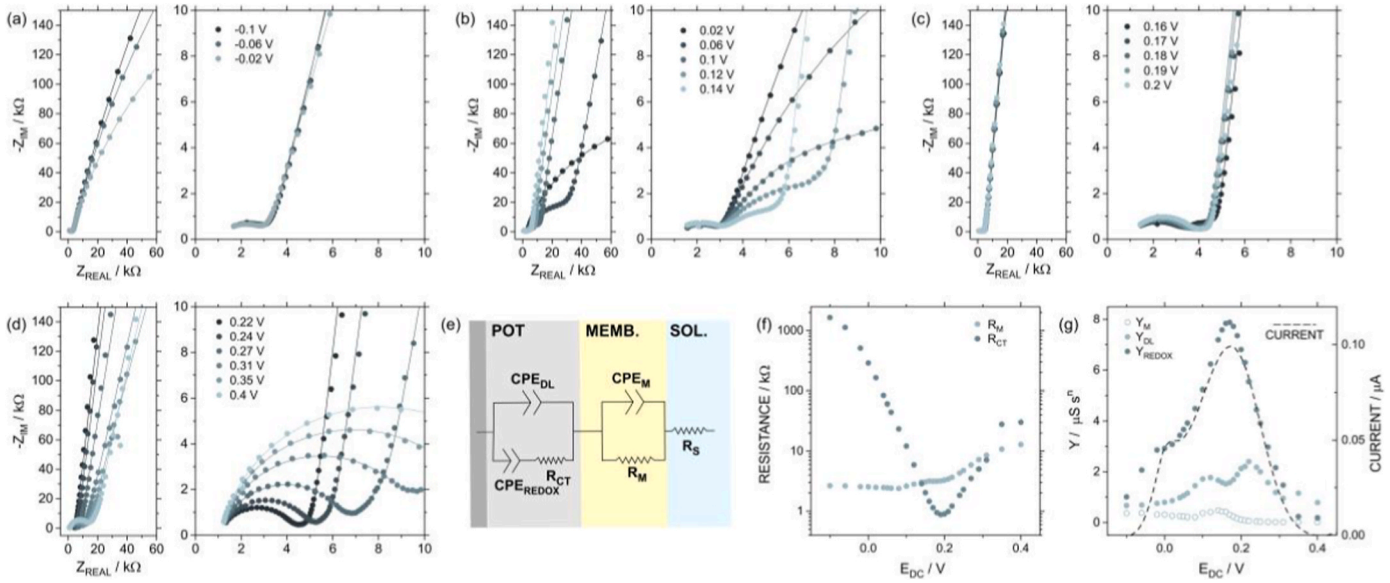

Fig. 2. EIS results. (a)–(d) Nyquist plots obtained at different E_{DC}. The left panels correspond to a wide impedance region, while the right panels represent a zoom-in. Lines correspond to the equivalent circuit model (ECM) fitting. (e) Scheme of the electrical equivalent circuit. CPE and R correspond to constant phase elements and resistances, respectively. Sub-index: DL, CT, M, and S refer to double-layer, charge transfer, membrane, and solution, respectively. (f) Resistances and (g) Y obtained from the ECM fitting at the different E_{DC}. In (g), the current corresponds to the background-subtracted current obtained by CV (scan rate 10 mV s^{-1}) for the same electrode in the same electrolyte. Supporting electrolyte: 10 mM NaCl. Electrode: GC/POT/MI.

carriers inside the film [56–58]. To further test this hypothesis, the MII film was deposited onto the GC/POT electrode to form GC/POT/MII. This membrane was similar as MI but with a reduced quantity of cation exchanger (half the amount). The EIS results demonstrated an equivalent response but with the Z_{REAL} semicircle intercept (between regions I and II) occurring around 4.2 kΩ, which was almost twice the value obtained for MI (~2.3 kΩ) (see Fig. S3). This result agrees with the expected loss of ion conduction capability due to the reduced cation exchanger concentration, and reinforces the hypothesis that Region I provides information about the membrane resistance [59].

Region II exhibited a predominantly capacitive behavior, corresponding to the total charge stored within the system. The redox reaction contribution was negligible due to the low E_{DC}, and therefore, the total charge was mainly associated with non-faradaic contributions such as the double-layer capacitance of the electrode-solution interface. It is worth mentioning that the $-Z_{IM}$ increment did not form a straight line of 90° with the x-axis, which indicates that the capacitive behavior is not ideal. This is in principle expected as different sources of non-ideality can arise in complex systems as the one studied herein (e.g., film roughness, inhomogeneities, or small contributions of redox reactions).

As E_{DC} approached $E_{1/2}$, the EIS results in Region I were maintained without any significant change. However, the low-frequency capacitive trend began to bend progressively, and within the potential range of 0.04 V < E_{DC} < $E_{1/2}$, a new semicircle emerged between Regions I and II. This feature can be observed in Fig. 2b and indicates the appearance of a new region in the EIS spectra that, based on its evolution with E_{DC}, can be attributed to the faradaic signal associated with the ET–IT coupling. Not only in Fig. 2b but also in Fig. 2c, it is observed how the semicircle decreased its size as E_{DC} approached the peak region. Once the E_{DC} value was within the peak region (0.15–0.20 V), the semicircle in Region II due to ET-IT was found to further decrease, while those in Region I, because of the membrane resistance, began to slowly increase their size.

At 0.19 V, both semicircles seemed to merge into only one. In principle, the semicircle due to ET-IT should exhibit its minimum size at $E^{0'}$ (which should be almost the same as $E_{1/2}$), as predicted by the theory for modified electrodes with thin redox films [54]. In the present system, the merging between both semicircles makes it difficult to evidence this trend; however, $E^{0'}$ should be in the range of ca. 0.18–0.2, which agrees with the peak position observed in the CV experiments (Fig. S1). At E_{DC}> 0.2 V, the Nyquist plot was characterized by only one semicircle that increased its diameter as E_{DC} increased, as presented in Fig. 2d. Finally, at E_{DC} = 0.6, the semicircle diameter exceeded 60 kΩ (Fig. S4). This could be attributed to the expulsion of most of the Na^+ ions, which is coupled to the redistribution of the lipophilic cation exchanger toward the polymer/membrane interface during POT oxidation. As a consequence, large regions of the sensing membrane become depleted of mobile ionic charge carriers, leading to a pronounced increase in membrane resistance. More in detail, the decrease in the ET-IT semicircle diameter as E_{DC} approached $E^{0'}$ can be explained by the ratio between oxidized/reduced POT species approaching 1. Thus, the redox contribution is maximized. In an ideal scenario, for each unity of POT that is oxidized, a positively charged site is generated, and one of the charge carriers in the film (Na^+ ion) is lost. Overall, the replacement of mobile Na^+ by fixed POT charges diminished the membrane's capacity to transport charge, increasing its resistance, which in turn yielded an increase in the semicircle diameter.

While EIS provides a significant amount of information, this is not always available in a straightforward manner. One of the traditional methods for extracting quantitative information is to fit experimental results to a suitable equivalent electrical circuit model (ECM). This was performed with our EIS results, with the results being provided in Fig. 2e. The proposed equivalent circuit is composed of an R_S representing the solution resistance, and that is placed in series with two parallel RQ, where R represents the resistance and Q denotes the constant phase elements (CPE). The first RQ component is related to membrane features: in essence, the membrane bulk CPE (CPE_M) and resistance (R_M) [60]. The second RQ component introduces the ET-IT phenomenon, and it is composed of the charge transfer resistance (R_{CT}) and CPE of the membrane/solution interface (CPE_{DL}). Notably, there is a clear complexity underlying the R_{CT} parameter. In the system under study, R_{CT} reflects not only the electronic transfer at the POT/electrode interface, but also ion transport within the membrane towards the POT/membrane interface, as well as ion fluxes at the membrane/solution interface, which occur to maintain electroneutrality and depend on the type of redox process (e.g., oxidation or reduction). Ion transport appears to be one of the dominant contributors to the magnitude of the resistance [48]. Finally, a redox CPE (CPE_{REDOX}) is placed in series with the R_{CT} to account for charge saturation in the EIS spectrum. Notably, the CPEs were used as replacements for capacitors to consider different sources of non-ideality, such as film inhomogeneity. In contrast to capacitors, CPEs are defined by the module Y and n. The n values range between 0.5 and 1, which is related to the capacitive behavior of the CPEs (see Table S1). It is worth noting that additional processes not included in the ECM may also influence the impedance response (e.g., interfacial phenomena); nonetheless, these cannot be resolved in the EIS spectra because associated impedances are much smaller than those of the dominant events included in our model. As demonstrated in previous reports, advanced analysis methods such as the distribution of relaxation times could make it possible to detect them [45].

In all the cases, the ECM well fitted the experimental results, as suggested by $\chi < 0.01$. As expected for thin-layer systems, R_{CT} demonstrated a "ν"-like shape in terms of E_{DC}, with a minimum value of 0.86 kΩ at 0.19 V (see Fig. 2f) [54]. Then, when E_{DC} approaches $E^{0'}$, the resistance involved in the redox transference shows its minimal value, demonstrating more facility to occur. The Y module related to the CPE_{REDOX} (Y_{REDOX}) also showed the typical peak in terms of E_{DC} expected for a thin-layer redox film, with a maximum value of 7.91 μS s^n at 0.17 V (see Fig. 2g). Overall, it followed the same trend as that observed for the current in the CV. As already mentioned, the double-peak was also evidenced in the CV recorded at low scan rates (10 mV s^{-1}).

Considering that the membrane resistance partially depends on the number and nature of charge carriers, the analysis of the R_M revealed more information about the ion transfer. At bias voltages below the peak potential, R_M remained constant with a value of 2.60 ± 0.05 kΩ (considering the values obtained at −0.1, −0.06, and −0.02 V, see Fig. 2f). As E_{DC} approached to $E_{1/2}$, R_M began to progressively increase, showing, for example, a magnitude of 3.18 kΩ at 0.19 V (estimated error in the fitting ~3 %). When E_{DC} exceeded $E_{1/2}$, R_M acquired a high resistance state. For instance, an R_M of 12.85 kΩ was estimated at 0.4 V (with a fitting error of 3.5 %), increasing further to 40 kΩ at E_{DC} = 0.6 V (more than 15 times the value at −0.1 V). It is worth mentioning that, at $E_{DC} \geq 0.6$ V, where the electrode resistance became relatively high, the quality of the EIS data deteriorated and became more complex. Thus, an additional RQ element was required in the fitting, as presented in Fig. S4.

Overall, the ECM analysis demonstrated the possibility of separating and quantifying different contributions occurring at different characteristic frequencies. However, it also manifested a disadvantage. The complexity of the phenomena makes in some cases the fitting in terms of ECM very challenging. In particular, the partial overlapping of different resistive and capacitive contributions makes it difficult to obtain reliable magnitudes with acceptable error values. For instance, the percentual fitting errors of parameters such as R_{CT} (where its contribution became minimal compared to R_M) in the peak region reached values of 25 %. In this context, our group introduced the use of DRT analysis for obtaining resistance values with a relatively simple mathematical inversion [45]. This method has been proven to be very useful to obtain different resistive values and to assist the subsequent ECM fitting [61]. Unfortunately, the analysis for these systems exhibiting thin-layer behavior is only reliable at high/moderate frequencies due to the divergent behavior of Z at low frequencies.

Another approach to attain information from EIS data is through the analysis of time constants. Although this method provides a more qualitative estimation of the system's resistances and capacitances, it can yield highly valuable insights into the processes occurring within the electrochemical cell. To investigate the characteristic times of the different processes, a common method is to identify the breaking points, i.e., the frequencies at which the system transitions from a resistive (frequency-independent) behavior to a capacitive one, and vice versa [42,44]. These points correspond to the frequencies where the phase angle reaches 45°. As shown in Fig. 3, at an $E_{DC} < -0.1$ V (well below the peak region), the breaking point associated with the transition from resistive behavior due to R_M to charge saturation appeared at ~135 Hz. This value decreased to ~13 Hz for the analogous transition at an $E_{DC} < 0.4$ V (above the peak potential) due to the higher system resistance. Conversely, at an E_{DC} of 0.19 V, where the transition corresponded to the change from resistive behavior due to R_{CT} to charge saturation, the breaking point was located at ~5 Hz. This finding indicates that the characteristic frequency associated with R_M, reflecting the dynamics of charge carriers and ions within the membrane, was significantly higher (and therefore, more rapid) than that of electron transfer.

So far, it has been demonstrated that EIS offers several advantages due to its ability to separate different phenomena occurring at distinct frequencies. The method requires relatively long measurement times (ca. 2 min per E_{DC} value) and, unlike other traditional electrochemical techniques such as CV, the information is not directly accessible. As an intermediate approach bridging the deconvolution of electronic and ionic phenomena with the need for shorter and simpler measurements, we applied AC voltammetry. This technique combines the principles of EIS and traditional voltammetry: the E_{DC} is swept with a staircase function while a low-amplitude AC voltage (typically 5–25 mV) is superimposed. The results are usually represented as the pulse current (PULSE I(AC)) as a function of E_{DC} bias voltage. In the case of the POT-membrane system here investigated, the E_{DC} scan allows control over the redox state of POT and, simultaneously, the coupled ET-IT processes, while the chosen frequency of the superimposed AC voltage enables selectively focusing on specific phenomena (faradaic or non-faradaic).

As shown in Fig. 4a, the AC voltammograms (ACV) were highly sensitive to the frequency of the AC perturbation. At low frequencies (e.g., <10 Hz), the signal was characterized by a relatively small and constant background current with a prominent peak around ~0.2 V. As the frequency increased, this peak gradually diminished, and the ACV adopted a sigmoidal shape, transitioning from high pulse currents at $E_{DC} < 0$ V to very low pulse currents $E_{DC} > 0.4$ V. As illustrated in Fig. S5, at frequencies above 1 kHz, the peak was nearly absent. Then, at frequencies exceeding 10 kHz, the sigmoidal response was also lost, with the pulse current remaining essentially constant across the E_{DC} range. For frequencies above 1 kHz, noise contributions became significant and therefore, measurements were typically conducted within the range of 3–5 Hz to 1 kHz.

According to the obtained results, it is hypothesized that the application of an AC voltage of low frequency (e.g., <10 Hz) led to an AC-voltammogram with a main contribution of the coupled ET-IT process. This is because the frequency is low enough to allow the POT redox reaction (with the concomitant IT transfer) to follow the sinusoidal perturbation and contribute to the signal. The signal is mainly characterized by a peak located at the same voltage as in the traditional CV (Fig. 4b). In contrast, the application of an AC voltage of high frequency (e.g., 250 Hz) led to an AC-voltammogram mainly determined by the number of charge carriers inside the membrane, which is in turn closely related to the IT process. This is explained by the fact that the sinusoidal perturbation oscillated with a frequency that fairly exceeded the characteristic frequency where the redox reaction occurs. Effectively, mainly phenomena related to ion transport in the membrane (and in the solution) can follow the AC voltage. Thus, the high amount of charge carriers in the membrane when $E_{DC} \ll E_{1/2}$ (i.e., where POT was mainly in a reduced state) generate minimal values of R_M, enabling a high PULSE I (AC) state. The oxidation of POT, with the concomitant ion transfer from the membrane to the solution phase, imposed a high resistive layer on the electrode that explained the low PULSE I(AC) state at $E_{DC} >> E_{1/2}$. Then, the transition between the high and the low PULSE I(AC) states was in the peak region of the CV. Moreover, the disappearance of the sigmoidal shape in ACV at frequencies above 10 kHz can be attributed to the fact that these frequencies substantially exceeded the characteristic value of ion transport in the membrane, causing the contribution of R_M to the signal to be lost (Fig. S5).

A feature that enables the use of thin-layer SC-ISEs as sensing platforms is the close relationship between the peak potential and the affinity of the membrane components towards the ion or, the tendency of the ion in question to enter the membrane from the solution. Regarding this latter and considering the GC/POT/MI electrode, the use of a supporting electrolyte based on a highly lipophilic cation such as tetrabutylammonium (TBA^+) gave rise to a big shift in the peak potential compared to the value obtained for Na^+ (Fig. 5a) [26,62]. Specifically, the mixture of NaCl and TBACl resulted in a voltammogram with two peaks located at 0.19 V and 0.53 V due to the interfacial transfer of Na^+ and TBA^+, respectively. The higher value in the peak potential for the TBA^+ is explained by the higher lipophilicity with respect to Na^+,

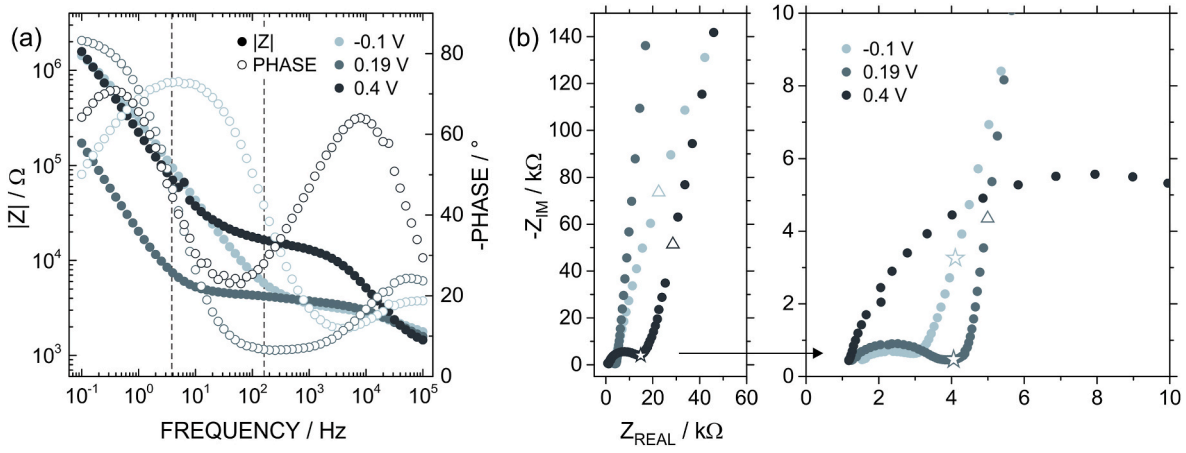

Fig. 3. (a) Bode and (b) Nyquist plots at three selected E_{DC} values for the same electrode and at the same conditions as those used in the experiments shown in Fig. 2. Dashed lines in Figure (a) indicate the breaking points arising from the transition from the resistive to the capacitive behavior for the EIS recorded at −0.1 V and 0.19 V. The frequencies of the breaking points are indicated as a star (at −0.1 V, in the absence of electron transfer) and a triangle (at 0.19 V, in the presence of ET-IT) in the Nyquist plots of Figure (b). Supporting electrolyte: 10 mM NaCl. Electrode: GC/POT/MI.

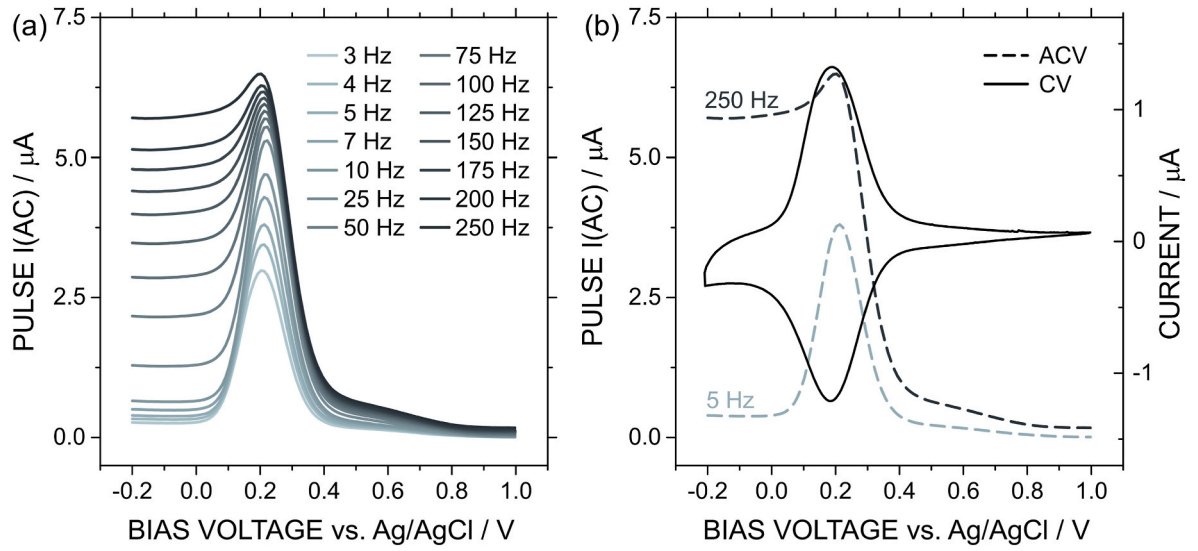

Fig. 4. (a) ACVs at different frequencies. (b) Overlapping of ACVs at 5 Hz and 250 Hz and the CV obtained with the same electrode. Supporting electrolyte: 10 mM NaCl. Electrode: GC/POT/MI.

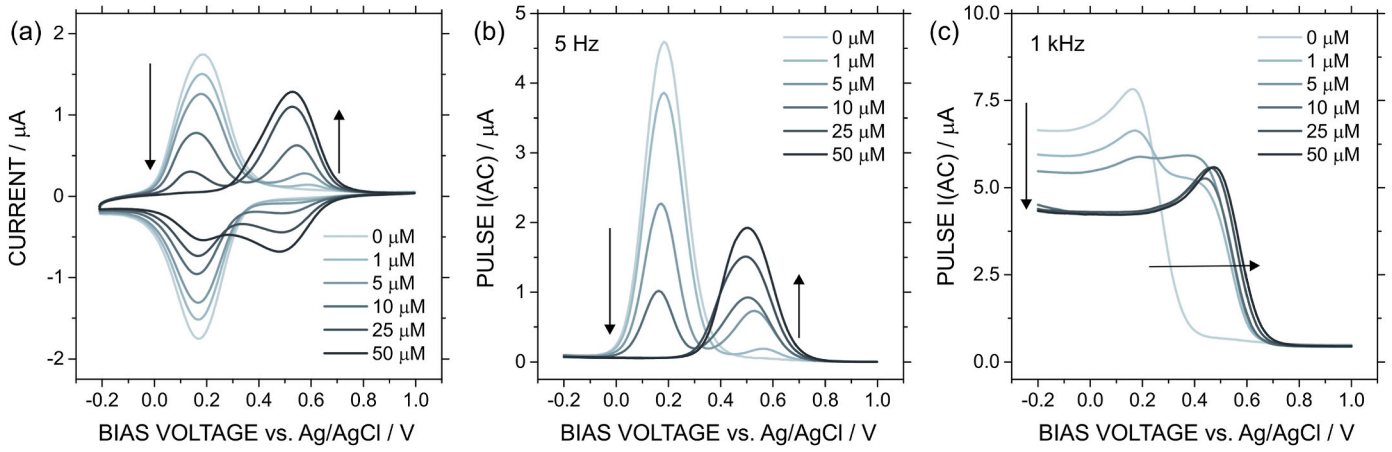

Fig. 5. (a) CV, (b) ACV at 5 Hz, and (c) ACV at 1 kHz obtained at different TBACl concentrations. Supporting electrolyte: 10 mM NaCl. Electrode: GC/POT/MI.

requiring, in turn, a higher potential to be released from the membrane. Increments in the TBA^+ concentrations (from 1 to 50 µM) generated an increase in the peak current and area, whereas a decrease in the Na^+ peak until disappearance (at 50 µM). Thus, the presence of different ions was evidenced as separated peaks, with the current magnitude and voltammetric charge correlating with the ion concentration in the sample solution (Fig. S6).

Considering ACV at a low frequency of 5 Hz, the response was characterized by prominent peaks, as explained for the case of only NaCl (Fig. 5b). Similar as the CV results, the peak maxima for the Na^+ and TBA^+ were located at 0.19 V and 0.53 V, respectively, with current intensities determined by the concentration of TBA^+ in the solution (Fig. S6). Then, the increment of the lipophilic cation concentration gave rise to an increment in its current peak while producing a decrease in the peak related to Na^+. As in the CV experiments, the trend observed for the peak current for the TBA^+ did not exhibit a clear linear relationship in the range from 1 to 50 µM. Notably, previous reports demonstrated that the linear range can be tuned by investigating different aspects of the system, e.g., adjusting the amount of cation exchanger, which is outside the scope of the present work [63,64].

The increment of the frequency up to 1 kHz was found to dramatically change the ACV features, as presented in Fig. 5c. The peaks were partially hidden, and the trend was mostly characterized by a step shape of PULSE I(AC) in terms of the voltage. Specifically, in the absence of TBA^+, at $E_{DC} < 0$ V, PULSE I(AC) remained relatively constant at a value of 6.634 ± 0.003 µA. While the trend was the same in the presence of TBA^+, the magnitude of PULSE I(AC) decreased a 35 %, reaching a value of 4.27 ± 0.01 µA. This agrees with the increment in R_M obtained in the EIS measurement at −0.1 V (Fig. S7). When the bias voltage approached the value corresponding to the Na^+ and TBA^+ transfers, PULSE I(AC) displayed an abrupt decrease. Remarkably, for TBA^+ concentrations of 1 µM and 5 µM, the ACV presented both steps, as expected due to the contribution of both cations to the total ET-IT mechanism. TBA^+ concentrations >10 µM presented only one step located at 0.59 V (considering the half-height), which agrees with the position of the TBA^+ peak in the CV. Finally, for $E_{DC} > 0.6$ V, PULSE I(AC) again kept relatively constant with a current value of 0.4397 ± 0.003 µA (less than 10 % difference among the different TBA^+ concentrations). As was mentioned for the Na^+ case, this behavior can be explained due to the different timescales of the involved procedures in the electrode during the direct voltage sweep.

Overall, ACV at low frequencies (e.g., 5 Hz) enables focusing on the complete ET-IT process (like the traditional CV), because both ET and IT are rapid enough to follow the low-frequency change in the AC voltage. However, when the AC voltage is modulated at frequencies higher than 250 Hz, ET cannot follow the sinusoidal perturbation and, therefore, its

contribution to PULSE I(AC) is limited. Under these conditions, the signal was mostly determined by the variations in the contribution of non-faradaic processes to the AC signal at the different E_{DC}, such as R_M. Considering that R_M is determined by the number of charge carriers inside the membrane, among other variables, the signal at high frequencies was again mostly related to the IT process.

Importantly, it is also possible to design highly selective membranes by including an ionophore, *i.e.*, a lipophilic molecule with a high affinity towards a certain ion [39]. This strategy has been employed in most of the potentiometric and voltammetric ion-selective electrodes. Considering the scope of this work, one question that arises is related to the possibility of using ACV to study the ET-IT phenomenon but also, to shed light on its analytical potential. In this context, Fig. 6a shows CVs at 100 mV s^{-1} in 10 mM NaCl without and with 150 μM of KCl for GC/POT/-MIII, an electrode modified with a membrane additionally containing the K^+ ionophore valinomycin.

In the absence of KCl, the CV displayed a single broad peak (full-width half-maximum FWHM of 0.26 V) with a maximum located at 0.48 V, due to the coupling of ET and IT from POT and Na^+ ions, respectively. While the nature of the cation exchanger did not change, the Na^+ peak was shifted by ~0.3 V compared to the membrane without the ionophore. This fact could suggest an enhanced stability of the ions in the lipophilic environment of the membrane due to the interaction of Na^+-ionophore-cation exchanger, making it necessary to apply higher voltages to trigger the IT. In the presence of 150 μM KCl, the CV also demonstrated a single peak but shifted at higher potentials compared to the case in the absence of KCl (Fig. 6a). Considering the relatively high concentration of KCl, this peak can be attributed to the coupling of ET and IT from POT and K^+ ions, respectively. As demonstrated in previous works, while the concentration of K^+ is 60 times lower than that of Na^+, the outstanding affinity of the valinomycin ionophore towards potassium strongly favors the entrance of this ion into the membrane over Na^+. This higher affinity also accounts for the higher peak potential of 0.75 V for the K^+ IT compared to those obtained for Na^+.

A similar trend was observed by performing ACV at a low frequency of 5 Hz (Fig. 6b). The ACV was characterized by a well-defined peak that shifted its position from 0.53 V to 0.73 V in the absence and presence of 150 μM K^+, respectively. When the frequency of the superimposed voltage was >250 Hz, the single peak was hidden, and a sigmoidal shape characterized the ACV. The response displayed a high PULSE I(AC) at bias voltages below $E_{1/2}$, followed by a sharp decrease in the current around $E_{1/2}$ and a low PULSE I(AC) state for bias voltages > $E_{1/2}$. Considering the frequency of perturbation, this feature is mainly due to the changes in R_M promoted by the ion transfer. Therefore, the addition of K^+ generated two main changes: (i) it shifted the transition from the high current state to the low to higher bias voltages, and (ii) it decreased the PULSE I(AC) values in the high current state. The first one is due to the higher voltages required to expel K^+ from the membrane to the solution and, consequently, the higher voltage required to transition from an ion-conductive membrane to an insulator one. The second one is related to the mobility of the ions inside the membrane. The saturation of the membrane with K^+ gave rise to R_M, which could indicate a lower mobility of K^+-valinomycin compared to the saturated membrane with sodium [56,65].

All the trends observed and explained in the ACVs can be rationalized by analyzing the EIS at different E_{DC} (Fig. 6c and d). The EIS at −0.1 V in the absence and presence of K^+ exhibited very similar features, but with a 50 % increase in the semicircle diameter (in Z_{REAL}) for the K^+ case, due to the increment in R_M promoted by the lower mobility of the complexed potassium ions (Fig. 6c).[9] At $E_{DC} = E_{1/2,Na+}$, the Nyquist plot in the absence of K^+ showed the appearance of a second semicircle at moderate/low frequencies ascribed to the R_{CT} of the ET-IT phenomenon. Conversely, at the same voltage but in the presence of 150 μM of K^+, the Nyquist plot showed the semicircle only at very low frequencies, accounting for a process with a very high R_{CT}. This is explained by the higher voltage required for the ET-IT phenomenon when the membrane is saturated with K^+. Thus, at $E_{DC} = E_{1/2,Na+}$, the response of the membrane saturated in K^+ presented a negligible contribution of charge transfer phenomena. At $E_{DC} = E_{1/2,K+}$, the Nyquist plot in the absence of K^+ exhibited only a big semicircle, indicating an increase in R_M associated with the decrease of mobile ion number inside the membrane (Na^+ release) (Fig. 6d). In the presence of K^+, the EIS response shows a small semicircle, likely due to the merging of R_M and R_{CT}. Finally, at $E_{DC} = 1.1$ V, both cases demonstrated an EIS response governed by a big semicircle due to the very high R_M (Fig. 6d).

Beyond fundamental studies, a potential application of the ACV technique could be related to analytical sensing. Fig. S8 presents the voltammetric response of GC/POT/MIII, comparing conventional CV with ACV at five different frequencies (3, 5, 10, 50, and 250 Hz). As observed, with increasing K^+ concentrations, both conventional CV and ACV at a frequency <50 Hz showed a decrease in the Na^+ peak, as well as an enhancement of the K^+ peak (Fig. S7a–h). This trend continues until K^+ accumulation reaches a point where only its peak is detected (concentration of 10 μM), which is due to membrane saturation. While in the CV both peaks were evidenced for a K^+ concentration of 10 μM, this was mainly due to the higher scan rate (100 mV s^{-1}) compared to those employed in the ACV (~8 mV s^{-1}) (Fig. S7b) [31]. As the frequencies increased beyond 50 Hz, however, the response transitioned from a peak-shaped to a sigmoidal profile. Concurrently, the increase in K^+ concentration caused a shift of the peak toward higher bias voltages, which can be attributed to the higher potential region where potassium ET–IT processes occur.

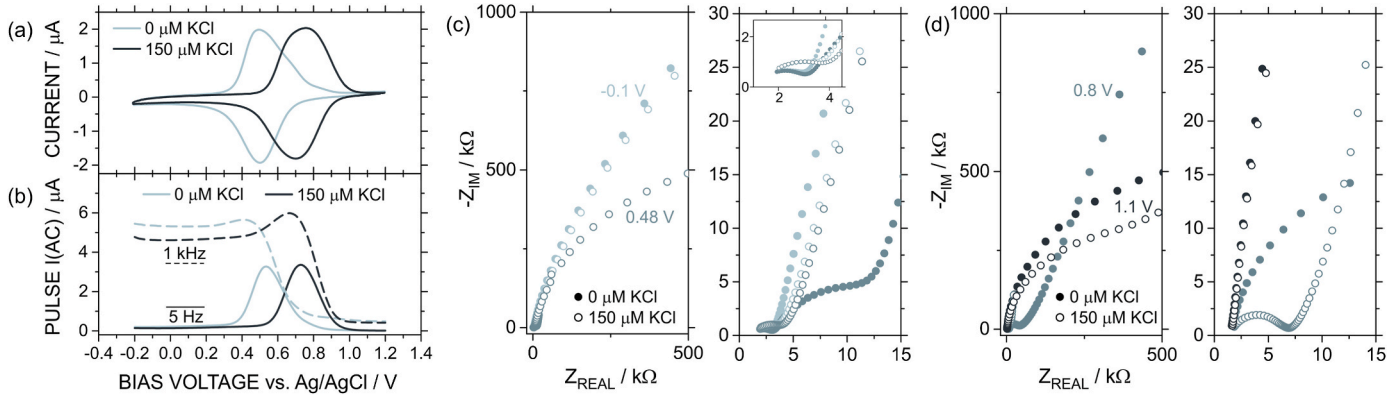

Fig. 6. (a) CV and (b) ACV at 5 Hz and 1 kHz, obtained in the absence and presence of KCl. (c) EIS at −0.1 V and 0.48 V ($E_{1/2,Na+}$), obtained in the absence and presence of KCl. (d) EIS at 0.75 V ($E_{1/2,K+}$) and 1.1 V, obtained in the absence and presence of KCl. In Figures (c) and (d), the left panel corresponds to the wide frequency spectra, while the right panel represents a zoom-in in the high-frequency/moderate frequency region. Supporting electrolyte: 10 mM NaCl. Electrode: GC/POT/MIII.

CV and ACV at low frequencies exhibited similar trends for the system under study. As shown in Fig. S9, while the use of ACV at low frequencies leads to peaks very well defined with a flat base, this does not seem to be translated into enhanced faradaic-to-background current ratios compared to the traditional CV. From a theoretical point of view, a conventional CV encompasses substantial contributions from both capacitive and faradaic processes; whereas ACV, through appropriate selection of perturbation frequency and amplitude, can generate signals dominated by faradaic components, which would be advantageous for sensing [54]. This behavior is analogous to that observed in differential pulse and square-wave voltammetry, as described in several electrochemistry textbooks [54]. For the system evaluated here, a frequency of 3 Hz is likely still too high to capture all the beneficial contributions, due to the uncompensated resistance introduced by the membrane. Nevertheless, further decrease in frequency would require a decrease in the scan rate, and therefore, an increase in analysis time. Also, the modulation of the amplitude could be key for improving the signal-to-noise ratio of ACV.

The possibility of detecting ions at subnanomolar concentrations in analogue systems to those evaluated in this article by employing CV has been demonstrated in previous reports [63,64,66]. Also, for thin-layer voltammetric electrodes, conventional CV offers a direct and reliable means of quantifying the total faradaic charge, a key parameter in the development of calibration-free sensors [28,36,67]. When combined with the possibility of operating at higher scan rates (thus reducing analysis times), these advantages suggest that the incremental benefit of employing more sophisticated voltammetric techniques beyond linear-scan CV and chronoamperometry may be limited in sensing applications of thin-layer ISEs. This conclusion is particularly relevant to the systems evaluated in this work, where the voltammograms are very flat and the subtraction of capacitive contributions in CVs does not pose a significant challenge.

In more complex scenarios such as multi-ion sensing or with electrode materials or configurations that provide complex background signals, ACV (an analogous pulse technique) may provide clear advantages [29,35]. In such cases, where different ions display distinct electron- or ion-transfer kinetics, frequency selection could serve as a powerful parameter to enhance or suppress specific ion contributions, thereby reducing peak overlap. Finally, it is worth noting that the present study employed a relatively low AC amplitude of 25 mV. Exploring higher amplitudes (50–100 mV) could enable the use of higher harmonic analysis and large-amplitude Fourier-transformed ACV, thereby further expanding the analytical opportunities of this approach [68,69].

4. Conclusions

This work provides new insights into the complex coupling between electron transfer and ion transfer in thin-layer all-solid-contact ion-selective electrodes, highlighting the potential of frequency-resolved techniques to rationalize the operation. By combining cyclic voltammetry, electrochemical impedance spectroscopy, and AC voltammetry, we quantitatively dissected the contributions of the different resistive and capacitive elements that govern sensor performance. While direct current techniques provide a response with accessible information about the faradaic and capacitive charge, obtaining deconvoluted information about the ET-IT process is not trivial. EIS analysis at different E_{DC} combined with the electrical equivalent circuit fitting revealed an alternative to separate the different phenomena. It allowed obtaining the membrane resistance, related to the total amount of ions and, consequently, influenced by the ion transfer, and the redox capacitance, related to the total amount of faradaic charge accumulated by the system. However, equivalent circuit fitting involved a challenging and time-consuming procedure. ACV proved to be an intermediate point to deconvolve processes occurring at different characteristic frequencies, such as ion transport and redox processes, in a simple and rapid way. When the frequency is relatively high, the response evidenced a sigmoidal shape that followed the same trend as R_M, demonstrating its relationship with the ion transfer procedure. These frequency-dependent trends were analyzed in three representative systems: (i) a membrane without ionophore in the presence of Na^+, (ii) a membrane exposed to mixed Na^+/TBA^+ solutions, and (iii) a valinomycin-containing (K^+-selective) membrane in the presence of Na^+ and K^+. In all the cases, ACV provided a direct means to distinguish the contributions of ion transfer (e.g., at 1 kHz) from the combined ET-IT phenomena (e.g., at 5 Hz). Although ACV may not initially appear to offer substantial advantages over simple CV from a sensing standpoint, it opens numerous opportunities for further exploration, including the use of higher harmonics and Fourier-transform-based analyses to gain a deeper mechanistic understanding.

CRediT authorship contribution statement

Gregorio Laucirica: Writing – original draft, Visualization, Validation, Software, Methodology, Investigation, Formal analysis, Data curation, Conceptualization. **Nuria Martínez-Lorca:** Writing – original draft, Visualization, Validation, Software, Methodology, Investigation, Formal analysis, Data curation, Conceptualization. **Gastón A. Crespo:** Writing – original draft, Visualization, Supervision, Methodology, Data curation, Conceptualization. **María Cuartero:** Writing – review & editing, Writing – original draft, Visualization, Supervision, Resources, Project administration, Methodology, Funding acquisition, Data curation, Conceptualization.

Declaration of competing interest

The authors declare the following financial interests/personal relationships which may be considered as potential competing interests: Maria Cuartero reports financial support was provided by European Research Council. Nuria Martinez-Lorca reports financial support was provided by Fundación Séneca. Gregorio Laucirica reports financial support was provided by Agencia Estatal de Investigación. If there are other authors, they declare that they have no known competing financial interests or personal relationships that could have appeared to influence the work reported in this paper.

Acknowledgments

This project received funding from the European Research Council (ERC) under the European Union's Horizon 2020 Research and Innovation Programme (grant agreement no. 851957). G.L. acknowledges the Grant JDC2023-051694-I funded by MICIU/AEI/10.13039/501100011033 and by the “ESF Investing in your Future”. N.M. acknowledges the support of a Fundación Séneca fellowship (22310/FPI/23) from Region de Murcia (Spain).

Appendix A. Supplementary data

Supplementary data to this article can be found at https://doi.org/10.1016/j.talanta.2026.129444.

Data availability

Data will be made available on request.

References

[1] Z. Yu, M. Xu, D. Wu, J. Qin, D. Tang, Do-it-yourself: an ultralow-cost sensing platform with integrated high-entropy nanozyme for the rapid detection of exhaled H 2 S, ACS Sens. 10 (2025) 7969–7976, https://doi.org/10.1021/acssensors.5c02530.

[2] R. Zeng, M. Qiu, Q. Wan, Z. Huang, X. Liu, D. Tang, D. Knopp, Smartphone-based electrochemical immunoassay for point-of-care detection of SARS-CoV-2

nucleocapsid protein, Anal. Chem. 94 (2022) 15155–15161, https://doi.org/10.1021/acs.analchem.2c03606.
[3] J.P. Hart, S.A. Wring, Screen-printed voltammetric and amperometric electrochemical sensors for decentralized testing, Electroanalysis 6 (1994) 617–624, https://doi.org/10.1002/elan.1140060802.
[4] E. Bakker, M. Telting-Diaz, Electrochemical sensors, Anal. Chem. 74 (2002) 2781–2800, https://doi.org/10.1021/ac0202278.
[5] S. Campuzano, P. Yáez-Sedeño, J. Pingarrón, Electrochemical affinity biosensors in food safety, Chemosensors 5 (2017) 8, https://doi.org/10.3390/chemosensors5010008.
[6] G. Maduraiveeran, W. Jin, Nanomaterials based electrochemical sensor and biosensor platforms for environmental applications, Trends Environ. Anal. Chem. 13 (2017) 10–23, https://doi.org/10.1016/j.teac.2017.02.001.
[7] E.T.S.G. da Silva, D.E.P. Souto, J.T.C. Barragan, J.de F. Giarola, A.C.M. de Moraes, L.T. Kubota, Electrochemical biosensors in point-of-care devices: recent advances and future trends, Chemelectrochem 4 (2017) 778–794, https://doi.org/10.1002/celc.201600758.
[8] S. Amemiya, Potentiometric ion-selective electrodes, in: Handb. Electrochem., Elsevier, 2007, pp. 261–294, https://doi.org/10.1016/B978-044451958-0.50020-3.
[9] R.P. Buck, Ion selective electrodes, Anal. Chem. 48 (1976) 23–39, https://doi.org/10.1021/ac60369a004.
[10] J. Bobacka, A. Ivaska, A. Lewenstam, Potentiometric ion sensors, Chem. Rev. 108 (2008) 329–351, https://doi.org/10.1021/cr068100w.
[11] W. Vonau, U. Guth, pH monitoring: a review, J. Solid State Electrochem. 10 (2006) 746–752, https://doi.org/10.1007/s10008-006-0120-4.
[12] M. Cuartero, G.A. Crespo, All-solid-state potentiometric sensors: a new wave for in situ aquatic research, Curr. Opin. Electrochem. 10 (2018) 98–106, https://doi.org/10.1016/j.coelec.2018.04.004.
[13] A. Michalska, All-solid-state ion selective and all-solid-state reference electrodes, Electroanalysis 24 (2012) 1253–1265, https://doi.org/10.1002/elan.201200059.
[14] J. Hu, A. Stein, P. Bühlmann, Rational design of all-solid-state ion-selective electrodes and reference electrodes, TrAC Trends Anal. Chem. 76 (2016) 102–114, https://doi.org/10.1016/j.trac.2015.11.004.
[15] J. Bobacka, Potential stability of all-solid-state ion-selective electrodes using conducting polymers as ion-to-electron transducers, Anal. Chem. 71 (1999) 4932–4937, https://doi.org/10.1021/ac990497z.
[16] J. Sutter, E. Pretsch, Response behavior of poly(vinyl chloride)- and polyurethane-based Ca 2+ -selective membrane electrodes with polypyrrole- and Poly(3-octylthiophene)-Mediated internal solid contact, Electroanalysis 18 (2006) 19–25, https://doi.org/10.1002/elan.200503373.
[17] J. Bobacka, M. McCarrick, A. Lewenstam, A. Ivaska, All solid-state poly(vinyl chloride) membrane ion-selective electrodes with poly(3-octylthiophene) solid internal contact, Analyst 119 (1994) 1985, https://doi.org/10.1039/an9941901985.
[18] G.A. Crespo, S. Macho, F.X. Rius, Ion-selective electrodes using carbon nanotubes as ion-to-electron transducers, Anal. Chem. 80 (2008) 1316–1322, https://doi.org/10.1021/ac071156l.
[19] M. Novell, M. Parrilla, G.A. Crespo, F.X. Rius, F.J. Andrade, Paper-based ion-selective potentiometric sensors, Anal. Chem. 84 (2012) 4695–4702, https://doi.org/10.1021/ac202979j.
[20] E.J. Herrero, B.K. Troudt, P. Bühlmann, The effect of paper on the detection limit of paper-based potentiometric chloride sensors, Anal. Chem. 94 (2022) 14898–14905, https://doi.org/10.1021/acs.analchem.2c02261.
[21] Q. Wang, Á. Molinero-Fernandez, J.R. Acosta Motos, G.A. Crespo, M. Cuartero, Microneedle sensors for ion monitoring in plants. One step closer to smart agriculture, ACS Sens. 10 (2025) 4771–4784, https://doi.org/10.1021/acssensors.5c01215.
[22] M. Parrilla, M. Cuartero, S. Padrell Sánchez, M. Rajabi, N. Roxhed, F. Niklaus, G. A. Crespo, Wearable all-solid-state potentiometric microneedle patch for intradermal potassium detection, Anal. Chem. 91 (2019) 1578–1586, https://doi.org/10.1021/acs.analchem.8b04877.
[23] M. Cuartero, G. Crespo, T. Cherubini, N. Pankratova, F. Confalonieri, F. Massa, M.-L. Tercier-Waeber, M. Abdou, J. Schäfer, E. Bakker, In situ detection of macronutrients and chloride in seawater by submersible electrochemical sensors, Anal. Chem. 90 (2018) 4702–4710, https://doi.org/10.1021/acs.analchem.7b05299.
[24] E. Bakker, E. Pretsch, Nanoscale potentiometry, TrAC Trends Anal. Chem. 27 (2008) 612–618, https://doi.org/10.1016/j.trac.2008.04.007.
[25] Y. Kim, S. Amemiya, Stripping analysis of nanomolar perchlorate in drinking water with a voltammetric ion-selective electrode based on thin-layer liquid membrane, Anal. Chem. 80 (2008) 6056–6065, https://doi.org/10.1021/ac8008687.
[26] Y. Kim, P.J. Rodgers, R. Ishimatsu, S. Amemiya, Subnanomolar ion detection by stripping voltammetry with solid-supported thin polymeric membrane, Anal. Chem. 81 (2009) 7262–7270, https://doi.org/10.1021/ac900995a.
[27] D. Kałuża, A. Michalska, K. Maksymiuk, Solid-contact ion-selective electrodes paving the way for improved non-zero current sensors: a minireview, Chemelectrochem 9 (2022), https://doi.org/10.1002/celc.202100892.
[28] Y. Liu, G.A. Crespo, M. Cuartero, Approaching to calibration-free ion detection based on thin layer coulometry with ultrathin ion-selective membranes, ACS Meas. Sci. Au 5 (2025) 63–69, https://doi.org/10.1021/acsmeasuresciau.4c00069.
[29] P.J. Greenawalt, S. Amemiya, Voltammetric mechanism of multiion detection with thin ionophore-based polymeric membrane, Anal. Chem. 88 (2016) 5827–5834, https://doi.org/10.1021/acs.analchem.6b00397.
[30] G.A. Crespo, M. Cuartero, E. Bakker, Thin layer ionophore-based membrane for multianalyte ion activity detection, Anal. Chem. 87 (2015) 7729–7737, https://doi.org/10.1021/acs.analchem.5b01459.
[31] D. Yuan, M. Cuartero, G.A. Crespo, E. Bakker, Voltammetric thin-layer ionophore-based films: part 1. Experimental evidence and numerical simulations, Anal. Chem. 89 (2017) 586–594, https://doi.org/10.1021/acs.analchem.6b03354.
[32] J. Guo, S. Amemiya, Voltammetric heparin-selective electrode based on thin liquid membrane with conducting polymer-modified solid support, Anal. Chem. 78 (2006) 6893–6902, https://doi.org/10.1021/ac061003i.
[33] H. Bao, J. Ye, X. Zhao, Y. Zhang, Conductive polymer nanoparticles as solid contact in ion-selective electrodes sensitive to potassium ions, Molecules 28 (2023) 3242, https://doi.org/10.3390/molecules28073242.
[34] P. Si, E. Bakker, Thin layer electrochemical extraction of non-redoxactive cations with an anion-exchanging conducting polymer overlaid with a selective membrane, Chem. Commun. (2009) 5260, https://doi.org/10.1039/b907893b.
[35] M. Cuartero, G.A. Crespo, E. Bakker, Ionophore-based voltammetric ion activity sensing with thin layer membranes, Anal. Chem. 88 (2016) 1654–1660, https://doi.org/10.1021/acs.analchem.5b03611.
[36] Y. Liu, G.A. Crespo, M. Cuartero, Voltammetric ion-selective electrodes in thin-layer samples: absolute detection of ions using ultrathin membranes, Anal. Chem. 96 (2024) 1147–1155, https://doi.org/10.1021/acs.analchem.3c04224.
[37] D. Yuan, M. Cuartero, G.A. Crespo, E. Bakker, Voltammetric thin-layer ionophore-based films: part 2. semi-empirical treatment, Anal. Chem. 89 (2017) 595–602, https://doi.org/10.1021/acs.analchem.6b03355.
[38] Z. Fan, E. Zamudio, Y. Liu, E. Laborda, A. Tillo, R. Sitdikov, G.A. Crespo, M. Cuartero, Adamantane Os(II) dissolved redox probe as an efficient ion-to-electron transducer for voltammetric ionophore-based sensing, Sensors Actuators B Chem 444 (2025) 138359, https://doi.org/10.1016/j.snb.2025.138359.
[39] R. Ishimatsu, A. Izadyar, B. Kabagambe, Y. Kim, J. Kim, S. Amemiya, Electrochemical mechanism of ion–ionophore recognition at plasticized polymer membrane/water interfaces, J. Am. Chem. Soc. 133 (2011) 16300–16308, https://doi.org/10.1021/ja207297q.
[40] Z. Qiu, D. Tang, J. Shu, G. Chen, D. Tang, Enzyme-triggered formation of enzyme-tyramine concatamers on nanogold-functionalized dendrimer for impedimetric detection of Hg(II) with sensitivity enhancement, Biosens. Bioelectron. 75 (2016) 108–115, https://doi.org/10.1016/j.bios.2015.08.026.
[41] J. Chen, P. Tong, L. Huang, Z. Yu, D. Tang, Ti3C2 MXene nanosheet-based capacitance immunoassay with tyramine-enzyme repeats to detect prostate-specific antigen on interdigitated micro-comb electrode, Electrochim. Acta 319 (2019) 375–381, https://doi.org/10.1016/j.electacta.2019.07.010.
[42] A.C. Lazanas, M.I. Prodromidis, Electrochemical impedance spectroscopy—a tutorial, ACS Meas. Sci. Au 3 (2023) 162–193, https://doi.org/10.1021/acsmeasuresciau.2c00070.
[43] S. Wang, J. Zhang, O. Gharbi, V. Vivier, M. Gao, M.E. Orazem, Electrochemical impedance spectroscopy, Nat. Rev. Methods Prim. 1 (2021) 41, https://doi.org/10.1038/s43586-021-00039-w.
[44] G. Laucirica, G.A. Crespo, M. Cuartero, Thin-layer behavior in carbon nanopipettes. Understanding the Iontronic-Electronic contributions, Anal. Chem. (2025), https://doi.org/10.1021/acs.analchem.5c02834.
[45] I. Robayo-Molina, G.A. Crespo, M. Cuartero, Usefulness of the distribution of relaxation time method in electroanalytical systems: the case of voltammetric ion-selective electrodes, ACS Omega 9 (2024) 8162–8172, https://doi.org/10.1021/acsomega.3c08656.
[46] B. Py, A. Maradesa, F. Ciucci, From theory to practice: unlocking the distribution of capacitive times in electrochemical impedance spectroscopy, Electrochim. Acta 479 (2024) 143741, https://doi.org/10.1016/j.electacta.2023.143741.
[47] S.O. Engblom, J.C. Myland, K.B. Oldham, Must ac voltammetry employ small signals? J. Electroanal. Chem. 480 (2000) 120–132, https://doi.org/10.1016/S0022-0728(99)00431-3.
[48] M. Cuartero, R.G. Acres, R. De Marco, E. Bakker, G.A. Crespo, Electrochemical ion transfer with thin films of Poly(3-octylthiophene), Anal. Chem. 88 (2016) 6939–6946, https://doi.org/10.1021/acs.analchem.6b01800.
[49] M. Cuartero, G.A. Crespo, E. Bakker, Polyurethane ionophore-based thin layer membranes for voltammetric ion activity sensing, Anal. Chem. 88 (2016) 5649–5654, https://doi.org/10.1021/acs.analchem.6b01085.
[50] Y. Liu, G.A. Crespo, M. Cuartero, Semi-empirical treatment of ionophore-assisted ion-transfers in ultrathin membranes coupled to a redox conducting polymer, Electrochim. Acta 388 (2021) 138634, https://doi.org/10.1016/j.electacta.2021.138634.
[51] Y. Liu, G.A. Crespo, M. Cuartero, Spectroelectrochemistry with ultrathin ion-selective membranes: three distinct ranges for analytical sensing, Anal. Chem. 94 (2022) 9140–9148, https://doi.org/10.1021/acs.analchem.2c01584.
[52] D.E. Stilwell, S. Park, Electrochemistry of conductive polymers: II . Electrochemical studies on growth properties of polyaniline, J. Electrochem. Soc. 135 (1988) 2254–2262, https://doi.org/10.1149/1.2096248.
[53] M.J. Honeychurch, G.A. Rechnitz, Voltammetry of adsorbed molecules. Part 1: reversible redox systems, Electroanalysis 10 (1998) 285–293, https://doi.org/10.1002/(SICI)1521-4109(199804)10:5<285::AID-ELAN285>3.0.CO;2-B.
[54] A.J. Bard, L.R. Faulkner, Electrochemical Methods. Fundamentals and Applications, second ed., Wiley, USA, 2001.
[55] E. Laviron, The use of linear potential sweep voltammetry and of a.c. voltammetry for the study of the surface electrochemical reaction of strongly adsorbed systems and of redox modified electrodes, J. Electroanal. Chem. Interfacial Electrochem. 100 (1979) 263–270, https://doi.org/10.1016/S0022-0728(79)80167-9.
[56] R.D. Armstrong, M. Todd, Ionic mobilities in PVC membranes, Electrochim. Acta 32 (1987) 155–157, https://doi.org/10.1016/0013-4686(87)87025-1.

[57] J.M. Zook, J. Langmaier, E. Lindner, Current-polarized ion-selective membranes: the influence of plasticizer and lipophilic background electrolyte on concentration profiles, resistance, and voltage transients, Sensors Actuators B Chem 136 (2009) 410–418, https://doi.org/10.1016/j.snb.2008.12.047.
[58] R.D. Armstrong, P. Nikitas, Transport of K+ in PVC matrix membranes containing valinomycin, Electrochim. Acta 30 (1985) 1627–1629, https://doi.org/10.1016/0013-4686(85)87008-0.
[59] C. Gabrielli, P. Hemery, P. Letellier, M. Masure, H. Perrot, M.-I. Rahmi, M. Turmine, Investigation of ion-selective electrodes with neutral ionophores and ionic sites by EIS. II. Application to K+ detection, J. Electroanal. Chem. 570 (2004) 291–304, https://doi.org/10.1016/j.jelechem.2004.04.007.
[60] K.N. Mikhelson, J. Bobacka, A. Lewenstam, A. Ivaska, Towards reversibility of ion transfer across the interface between valinomycin membranes and aqueous electrolyte solutions, Russ. J. Electrochem. 39 (2003) 771–776, https://doi.org/10.1023/A:1024834320728.
[61] A. Maradesa, B. Py, J. Huang, Y. Lu, P. Iurilli, A. Mrozinski, H.M. Law, Y. Wang, Z. Wang, J. Li, S. Xu, Q. Meyer, J. Liu, C. Brivio, A. Gavrilyuk, K. Kobayashi, A. Bertei, N.J. Williams, C. Zhao, M. Danzer, M. Zic, P. Wu, V. Yrjänä, S. Pereverzyev, Y. Chen, A. Weber, S.V. Kalinin, J.P. Schmidt, Y. Tsur, B. A. Boukamp, Q. Zhang, M. Gaberšček, R. O'Hayre, F. Ciucci, Advancing electrochemical impedance analysis through innovations in the distribution of relaxation times method, Joule 8 (2024) 1958–1981, https://doi.org/10.1016/j.joule.2024.05.008.
[62] E. Zdrachek, E. Bakker, Electrochemically switchable polymeric membrane ion-selective electrodes, Anal. Chem. 90 (2018) 7591–7599, https://doi.org/10.1021/acs.analchem.8b01282.
[63] K. Xu, G.A. Crespo, M. Cuartero, Subnanomolar detection of ions using thin voltammetric membranes with reduced exchange capacity, Sensors Actuators B Chem 321 (2020) 128453, https://doi.org/10.1016/j.snb.2020.128453.
[64] K. Xu, Y. Liu, G.A. Crespo, M. Cuartero, Ultrathin ion-selective membranes for trace detection of lead, copper and silver ions, Electrochim. Acta 427 (2022) 140870, https://doi.org/10.1016/j.electacta.2022.140870.
[65] R.D. Armstrong, A.K. Covington, G.P. Evans, Relative mobilities of ions in ion-selective electrodes with poly(vinyl chloride) membranes, Anal. Chim. Acta 166 (1985) 103–109, https://doi.org/10.1016/S0003-2670(00)84857-6.
[66] B. Kabagambe, M.B. Garada, R. Ishimatsu, S. Amemiya, Subnanomolar detection limit of stripping voltammetric Ca 2+ -Selective electrode: effects of analyte charge and sample contamination, Anal. Chem. 86 (2014) 7939–7946, https://doi.org/10.1021/ac501951m.
[67] Thin layer samples controlled by dynamic electrochemistry, Chimia 69 (2015) 203, https://doi.org/10.2533/chimia.2015.203.
[68] N.G. Baranska, B. Jones, M.R. Dowsett, C. Rhodes, D.M. Elton, J. Zhang, A. M. Bond, D. Gavaghan, H.O. Lloyd-Laney, A. Parkin, Practical guide to large amplitude fourier-transformed alternating current voltammetry—What, how, and why, ACS Meas. Sci. Au 4 (2024) 418–431, https://doi.org/10.1021/acsmeasuresciau.4c00008.
[69] J. Zhang, S.-X. Guo, A.M. Bond, Discrimination and evaluation of the effects of uncompensated resistance and slow electrode kinetics from the higher harmonic components of a fourier transformed large-amplitude alternating current voltammogram, Anal. Chem. 79 (2007) 2276–2288, https://doi.org/10.1021/ac061859n.